Droplet breakup in a model of the Hele-Shaw cell

Peter Constantin and Todd F. Dupont
Computational and Applied Mathematics Program, Ryerson Laboratory, The University of Chicago, Chicago, Illinois 60637

Raymond E. Goldstein
Department of Physics, Princeton University, Princeton, New Jersey 08544

Leo P. Kadanoff and Michael J. Shelley
Computational and Applied Mathematics Program, Ryerson Laboratory, The University of Chicago, Chicago, Illinois 60637

Su-Min Zhou
Department of Physics, The University of Chicago, 5640 South Ellis Avenue, Chicago, Illinois 60637
(Received 29 April 1992; revised manuscript received 24 November 1992)

The Hele-Shaw cell involves two immiscible fluids separated by an interface. Possible topology changes in the interface are investigated. In particular, we ask whether a thin neck between two masses of the fluid can develop, get thinner, and finally break. To study this, we employ the lubrication approximation, which implies for a symmetrical neck that the neck thickness h obeys $h_t+(hh_{xxx})_x=0$. The question is whether, starting with smooth positive initial data for h, one can achieve $h=0$, and hence a possible broken neck within a finite time. One possibility is that, instead of breaking, the neck gets continually thinner and finally goes to zero thickness only at infinite time. Here, we investigate one set of initial data and argue that in this case the system does indeed realize this infinite-time breakage scenario.

PACS number(s): 03.40.Gc, 47.20.Ky, 47.15.Hg

I. INTRODUCTION

One of the questions which runs through many mathematical studies of hydrodynamics and of nonlinear partial-differential equations (PDE's) is whether or not, starting from initially smooth flows, the solutions to these equations develop singularities in finite time. For example, understanding whether or not singularities develop in the Euler equations is quite important for the development of a good understanding of turbulence. Generally, these singularity questions have turned out to be very hard [1]. We do understand Burger's equation [2], which describes a one-dimensional fluid. However, we do not understand singularity questions related to Euler's equation in three dimensions [3].

One difficulty is that singularities may develop only occasionally or that they may be hard to observe. But, there is one class of problems in which the appearance of a singularity is likely to be almost unmistakable. Consider two fluids separated by an interface. Imagine that at the interface there is a discontinuous pressure drop Δp across the surface related to the surface tension τ through

$$\Delta p=\tau\sum_j R_j^{-1}\ , \tag{1}$$

where the R's are the principal radii of curvature of the surface. Clearly, if a thin neck connecting two regions of fluid suddenly breaks, the interfaces bounding the two separated fluids will tend to fly apart. Such events must involve the appearance of some singularity in the shape of the surface or the velocity or both. This neck breakage must occur if fluids are ever to separate into disconnected parts. Figure 1 is a sequence which shows such a breakage in a laboratory setup [4]. This figure shows a quasi-two-dimensional situation in which two fluids (air and water) are confined to the narrow gap between two glass plates. It is not clear how important a role the actual three-dimensional nature of the cell plays in the breakup of the mass of water.

In this paper, we shall not focus upon the experimental situation. Instead, we shall question when and how a given set of hydrodynamic equations can show neck breakage, with the accompanying singularity formation. In this paper, we propose to investigate this question in the simplest possible situation: the so-called Hele-Shaw [5] flow in which two fluids are confined to the thin gap region between two flat plates. The gap is thin so that the component of the velocity perpendicular to the plates may be neglected. The plates produce a friction upon the fluids so that their average velocity components along the plates $\mathbf{v}$ may be described by a potential flow. The two-component velocity obeys

$$\mathbf{v}=-\frac{b^2}{12\mu}\nabla p\ . \tag{2}$$

Here, the pressure p is presumed to depend only upon the coordinates x and y along the plates, b is the distance between the two plates, and μ is the viscosity of the fluid in question. For simplicity we assume that the two fluids have a very high viscosity contrast, as between pair air and water. Then the pressure within the less viscous fluid may be considered to be independent of position [6].

Common experience shows that separation of a mass of

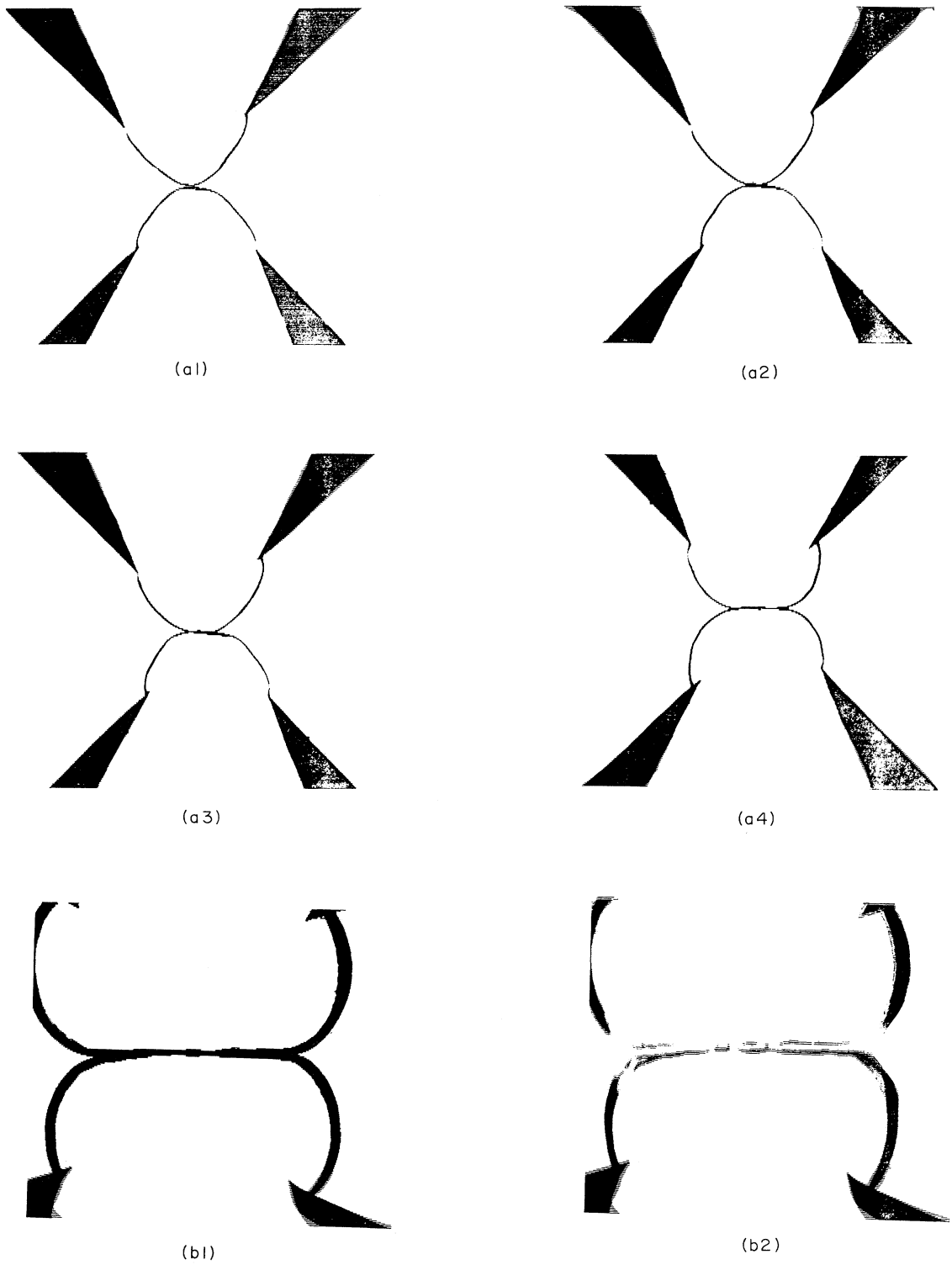

FIG. 1. From the experiments of Mason, Shyamsunder, and Goldstein. These pictures show the dynamics of the breakup of a mass of fluid in a cell which contains air and water trapped in the thin region between two glass plates. We view the situation through the plates. The white regions are fluids: air and water. These are kept apart by Teflon spacers, which appear in dark. The other dark area roughly marks the positions of the air-water interface. Refraction produces an apparent interface region much wider than the real interface. Because of the refraction, it is hard to judge the dimensions of the thin neck of water. However, the actual breakup occurs when the neck of water has transverse size which approaches the distance between plates. Consequently, the breakup may be a three-dimensional effect. (a) A thin neck connecting two masses of water has thinner and thicker potions. (b) The neck begins to break apart into separate drops.

fluid into two disconnected parts can easily occur in three dimensions. However, according to popular mythology [7], this separation may not always be possible in two dimensions. Specifically, it is far from clear that any such separation is permitted within the simplified two-dimensional hydrodynamic equations. Consequently, in this paper, we focus our attention upon the Hele-Shaw situation.

To fully define this situation, we must append to Eq. (2) boundary conditions describing discontinuities at the interface between the two fluids. One such boundary condition is the statement that the normal component of the velocities of both fluids is identical, so that the interface moves with the fluids. The other boundary condition is more problematical [8]. In the real world, fluids are three dimensional, and Eq. (1) contains two principal radii of curvature. However, since we are primarily interested in mathematical issues, we choose the simplest possible boundary condition. We take Eq. (1) to hold with R being the radius of curvature of the interface within the x-y plane. In this way, we get the simple Saffman-Taylor problem, the subject of many previous studies [9,10].

A. Derivation of lubrication approximation

But now we seek a further simplification. We shall argue that a variety of the well-known lubrication approximation [11] should be applicable to a sufficiently thin neck region. Imagine that a viscous fluid, "water," has formed a thin neck in preparation for its splitting into two parts (see Figs. 2 and 3). It is surrounded by "air" and the pressure of the "air" may depend upon time, but it is independent of position. Then, if the neck is thin enough, it is very implausible that we shall see a situation in which the curvatures on the two sides of the neck are different, as in Fig. 2. For in that case, the different curvatures on opposite sides of the neck would produce different pressures on opposite sides of the neck. A large flow would arise with the likely result of evening out the curvatures on opposite sides of the neck. For this reason, we assume that the neck is symmetrical as in Fig. 3. Then, the neck region can be described by a variable $h(x,t)$, where x describes distance along the symmetry line, t is the time, and $2h$ is the thickness of the interface at position x.

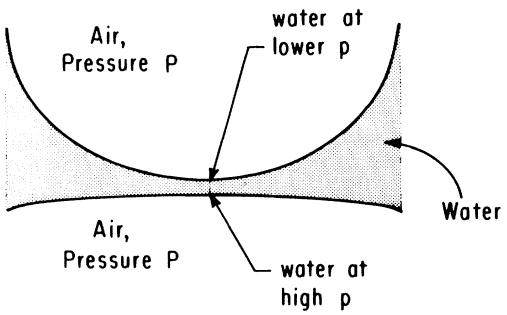

FIG. 2. The setup of the problem solved here. A thin neck is sketched. This is an asymmetrical case. This will produce a flow across the neck which tends to reduce the asymmetry.

The lubrication approximation is derived from the assumption that, because the interface is so thin, we need not consider the variation in the pressure in the y direction. Hence the flow is primarily parallel to x, and its speed is

$$v=-\frac{b^2}{12\mu}\partial_x p(x,t) . \tag{3}$$

The total current of particles j at the position x is velocity times height

$$j=vh . \tag{4}$$

Since the flow in the y direction is quite small, the continuity equation is the statement

$$\partial_t h+\partial_x j=0 . \tag{5}$$

One more equation is needed to complete the set. In the Saffman-Taylor approximation the pressure jump is given by the one-dimensional curvature, so that in place of Eq. (1) we have

$$\Delta p=\tau\frac{h_{xx}}{(1+h_x^2)^{3/2}} .$$

In the lubrication approximation, one takes h_x to be small and hence replaces the denominator in this expression by unity. In this way, one finds that the pressure inside the viscous fluid is given by

$$p=P(t)-\tau h_{xx} , \tag{6}$$

where $P(t)$ is the pressure applied to the less viscous fluid. Equation (2)–(6) may be combined into the single statement

$$h_t+(hh_{xxx})_x=0 . \tag{7}$$

Here we have defined the unit of time to be

$$t_0=\frac{12\mu}{b^2\tau} , \tag{8}$$

so that all dimensional factors drop out of Eq. (7). We shall study this equation in the remainder of this paper.

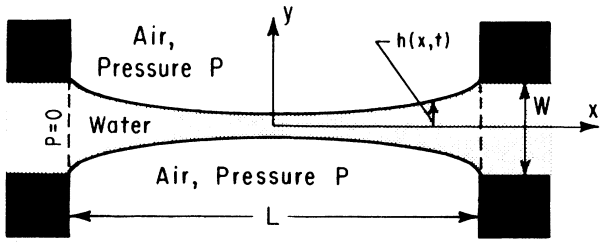

FIG. 3. The setup of the problem solved here. This is a symmetrical case. A schematic picture shows the system setup and boundary conditions. The heavy curves are walls which separate the two fluids. The length L is much much greater than length W. In this case we can equivalently imagine that there is a slip wall on the plane of symmetry. Our variable is $h(x,t)$.

There is one important physical effect left out of Eq. (7): gravity. Imagine there is an additional force on the viscous fluid which points toward negative x and is simply proportional to the volume of the fluid. This force produces an additional term in Eq. (7) of the form Vh_x, where V is the terminal velocity of an isolated drop of viscous fluid in the cell. This extra term may be eliminated by going into a coordinate system moving with speed V, but care must be taken in such Galilean transformations if the imposed boundary conditions break translational invariance.

B. Zeros imply singularities

We wish to ask whether Eq. (7) develops singularities in any finite time with generic starting data in which h is smooth and positive. Mathematically, the positivity of h is required for Eq. (7) to be meaningful, since the highest-order derivative terms in the equation have the structure

$$h_t + hh_{xxxx} = (\text{less singular terms}) . \tag{9}$$

Thus, if h is negative, the entire problem is ill posed in the sense of Hadamard [12]. As h goes to zero, one must develop singularities in x. To form this conclusion, assume that the starting data for h is smooth and positive. Then no singularity will arise until h becomes either zero or infinite someplace. Put the question about infinite h aside; it will not trouble us here. So ask what happens when h develops a zero. Let $x^*(t)$ be the position of the minimum of $h(x,t)$ in x. The minimum value of h at time t is $h_{\min}(t)=h(x^*(t),t)$, which in turn formally obeys

$$\frac{d}{dt}\ln(h_{\min}) = -W(t), \quad W(t)=h_{xxxx}(x^*(t),t) \tag{10}$$

according to Eq. (7). Therefore, if $h_{\min}$ is to approach zero at any finite time t_c, the fourth derivative of h must have a very strong singularity. In fact, the integral of $W(t)$ up to t_c must diverge. Thus a zero in $h(x,t)$ implies a singularity in the x dependence of h. Conversely, one can prove that as long as h is strictly positive it is nonsingular.

C. Outline of paper

The remainder of this paper is divided into two parts. In the next section, we first specify the model by giving boundary and initial data. The model is shown to be dissipative in the sense that an integral depending upon the solution decreases uniformly. Consequences of this decrease are discussed. Finally, two numerical methods, a finite-difference scheme and a Galerkin scheme, are described and explained in detail. The following section discusses the results of simulations. Long-term solutions are obtained and their scaling properties are described.

D. Further studies

The model problem discussed in this paper is still being studied. We believe that under appropriate initial and boundary conditions (but not the ones studied here) it is likely that there is singularity in finite time. A related paper that presents the supporting evidence for this view is in preparation.

II. SIMULATIONS AND SCALING ANALYSIS

We wish to produce a situation in which $h(x,t)$ will certainly go to zero, potentially producing a finite-time singularity. To achieve this, we imagined taking a column of fluid of finite thickness, and squeezing very hard upon it. How fast would the fluid flow out? Would $h_{\min}$ go to zero at finite time? Intuition suggests that squeezing should not be sufficient to break the column in finite time. Can we back this intuition with hard argument?

A. The model

We considered a finite interval $-1<x<1$ and insisted that the height remain one at the endpoints. We visualize that, in the more viscous fluid, the pressure is held to zero in the region of these end points (see Fig. 3). The other fluid is held at a nonzero pressure P. This situation is then represented by boundary conditions at the two end points

$$h(\pm 1,t)=1, \quad h_{xx}(\pm 1,t)=P(t) \tag{11}$$

for t greater than zero. Here $P(t)$ is a dimensionless version of the pressure in the "air." If $P>0$, the "air" is pushing on the "water." There is a tendency for the column of water to thin. If $P<0$, the column has a tendency to bulge at the center. The particular cases we studied all have $P(t)$ being a constant, independent of t. The problem is fully defined by giving P and initial data. At time zero, we take the height h to be unity:

$$h(x,0)=1 \tag{12}$$

for x in the basic interval $[-1,1]$.

B. A variational principle and its consequences

Equation (7) is dissipative in structure. Hence, one should expect that there might be some kind of Lyapunov function for this equation. Consider the integral

$$I[h]=\int_{-1}^{1} dx\left(\tfrac{1}{2}h_x^2+Ph\right) , \tag{13}$$

which is well defined up to the time of the first singularity. Here h is required to obey boundary conditions (11). If h and P are non-negative, this integral is non-negative. A brief calculation shows that Eqs. (7) and (11) imply that $I(t)$ has a monotonic decrease in time. Let $h(x,t)$ be a solution to Eqs. (7) and (11). After two integrations by parts, one calculates the rate of decrease of $I[h(\,,t)]$ to be

$$\frac{d}{dt}I=-K(t); \quad K(t)=\int_{-1}^{1} dx h_{xxx}^2 h . \tag{14}$$

Here $K(t)$ is well defined and positive for all times up to

t_c. The Lyapunov function character of h is established if we notice that Eq. (7) is equivalent to

$$\partial_t h(x,t)=\partial_x\left[h(x,t)\times\partial_x\left[\frac{\delta}{\delta h(x,t)}I[h(t)]\right]\right]. \quad (15)$$

Using these results, we can find all possible time-independent solutions of Eq. (7) using the boundary conditions (2.1). From Eq. (14), these solutions must h obey one of the two conditions:

$$\begin{aligned}&\text{(i)}h_{xxx}=0 \text{ (pressure independent of x) or}\\&\text{(ii)}h=0 \text{ (no fluid)}\end{aligned} \quad (16)$$

for all x save perhaps a set of measure zero. For $P<2$, the possible steady solution is one with constant h_{xx}, i.e.,

$$H_\infty(x)=1+P(x^2-1)/2 \text{ for } P<2 . \quad (17)$$

This height satisfies Eq. (7) and the boundary conditions [Eq. (11)]. Notice that this solution cannot apply for $P>2$ since then the height will be negative. For $P>2$, there is only one solution with non-negative h and continuous h_x which obeys Eq. (16) and our boundary conditions, namely

$$H_\infty(x)=\begin{cases}\frac{P}{2}(x-x_0)^2 & \text{if } x>x_0\\ 0 \text{ if } |x|<x_0 & \text{for } P>2\\ \frac{P}{2}(x+x_0)^2 & \text{if } x<-x_0 .\end{cases} \quad (18)$$

This solution has a discontinuity in h_{xx}, at $x=\pm x_0$, with

$$x_0=1-\sqrt{2/P} . \quad (19)$$

In this situation, the pressure is continuous except at $x=\pm x_0$, where the height is zero. Thus, Eq. (18) gives a type of weak solution to Eq. (7).

The functions H_∞ minimize the integral within the class of all non-negative functions with first-derivatives square integrable which obey the boundary conditions (11). They represent the likely infinite-time limit of the solutions, if no singularity intervenes in finite time.

Then, starting from a smooth and positive initial $h(x,0)$, it can be proved that, if $P<2$, then $h(x,t)\to H(x)=1+P(x^2-1)/2$.

If $P>2$ we expect that, if the solution exists for all time, it will approach the weak solution in which Eq. (7) is obeyed almost everywhere and has h_x continuous.

C. The simulational methodology

Solutions to Eq. (7) for h were constructed by using two different methods: a finite-difference scheme and a finite-element scheme.

1. Finite-difference method

The first numerical method we used was a finite-difference method with equally spaced mesh points between 0 and 1. It is a second-order, implicit method of the Crank-Nicholson type. The x derivatives in Eq. (7) are approximated by central differences involving a maximum of five mesh points.

We consider the case of solutions to Eq. (7) that are symmetric about $x=0$ (initial symmetry is preserved by the evolution). Discretizing the interval [0,1] by the $N+1$ equally spaced mesh points,

$$0=x_1<x_2<\cdots<x_{N+1}=1 .$$

The central difference formulas used are

$$\begin{aligned}&\delta u_{i,j}=(h_{i+1,j}-h_{i-1,j})/2\Delta x ,\\&\delta^2 u_{i,j}=(h_{i+1,j}-2h_{i,j}+h_{i-1,j})/\Delta x^2 ,\\&\delta^3 u_{i,j}=(h_{i+2,j}-2h_{i+1,j}+2h_{i-1,j}-h_{i-2,j})/2\Delta x^3 ,\\&\delta^4 u_{i,j}=(h_{i+2,j}-4h_{i+1,j}+6h_{i,j}-4h_{i-1,j}+h_{i-2,j})/\Delta x^4 .\end{aligned} \quad (20)$$

Here Δx is the mesh size in space. For h the index i indicates that the x coordinate is x_i, while j denotes the jth time level. We will keep this notation in this section. These central differences approximate the same order of partial derivatives with respect to x, with a leading error of order Δx^2.

The boundary conditions are specified as

$$\begin{aligned}&h_{N+1,j}=1 ,\\&(\partial_x^2 h)_{N+1,j}=P ,\\&(\partial_x^{(2k+1)}h)_{1,j}=0 \text{ for } k=0,1,2,\ldots ,\end{aligned} \quad (21)$$

where P is constant in our simulations.

The last two finite-difference formulas, when centered at x_N, require a value for h at $x_{N+2}=1+\Delta x$. We use the first two boundary conditions to provide a high-order extrapolation for this value by the formula

$$h_{N+2,j}=2h_{N+1,j}-h_{N,j}+P\Delta x^2 , \quad (22)$$

where $h_{N+1,j}$ is always 1 according to the first boundary condition. Equation (22) gives a fourth-order approximation to h at this extra mesh point. Thus, when we use Eq. (20) to compute up to fourth-order x derivatives at the Nth mesh point, we can keep the leading error of order Δx^2.

The last boundary condition, the symmetry condition, is used to compute the derivatives for the first and second mesh points. When we need to know values of h at points which sit on the negative x axis, we use their counterparts on the positive x axis.

To summarize, given the values of h on the N interior mesh points, together with the boundary conditions and Eq. (20), all the central difference approximations required for Eq. (7) can be evaluated at the interior mesh points with a leading error of order Δx^2.

Except at the first step, for the discretization in time we use a Crank-Nicholson-type implicit scheme, where the following finite-difference equation is used to approximate the original partial differential equation Eq. (7):

$$\begin{aligned}(h_{i,j+1}-h_{i,j-1})/\Delta t=&-h_{i,j}(\delta^4 h_{i,j+1}+\delta^4 h_{i,j-1})\\&-\delta h_{i,j}(\delta^3 h_{i,j+1}+\delta^3 h_{i,j-1}) ,\end{aligned} \quad (23)$$

where Δt is the time step between these three time levels. For smooth $h(x,t)$ the leading error for this time discretization is of order Δt^2. Using Eq. (23) we can get $h_{i,j}$ from information of two previous time levels $h_{i,j-1}$ and $h_{i,j-2}$.

To get h at time Δt, we use a central difference formula [see Eq. (20)] to compute $-(hh_{xxx})_x$ and an explicit Euler step to get h at time $\Delta t/2$. We then use Eq. (23) to get h at time Δt from h at time 0 and time $\Delta t/2$ (here the time step is $\Delta t/2$). After getting h at time Δt, we iterate Eq. (23) to update h to the next time level with time step Δt. Each time we advance h, we will check if the new minimum value of h is less than $\frac{1}{2}$ that of the previous time. If the minimum value of h decreases too fast, we will halve the time step Δt. We stopped our program when Δt was less than 10^{-12}.

Equation (23) with boundary conditions Eq. (21) can be written as N linear equations for $h_{i,j+1}$ $(i=1,2,3,\ldots,N)$ with a banded coefficient matrix whose width is 5. These linear equations are solved by Gaussian elimination. The stability of this elimination method requires that Δt be of order Δx^4.

As will be seen shortly, numerically computed solutions to Eq. (7) can evince nearly singular behavior, and we found a problem in using a uniform mesh in space. At later times we did not have a small enough mesh size around the minimum point of h to adequately resolve the diverging terms h_{xxx} and h_{xxxx}, while for other parts of the solution we had more than enough mesh points. If we add more mesh points to get good resolution around the minimum point of h, the time step has to be very small (decreases like Δx^4) in order to satisfy the stability requirement. So we turned to another second-order scheme—a Galerkin method—which is easier to implement when the mesh is not uniform.

2. *Galerkin method*

We have used a conventional Galerkin method to approximate solutions of Eq. (7) with boundary condition [Eq. (11)]. The basis of the Galerkin method is the following integral identity. For v a continuously differentiable piecewise polynomial function vanishing at $x=\pm 1$, the solution h satisfies

$$\int_{-1}^{1}[h_t v+h_{xx}(hv_x)_x]dx=Pv_x|_{-1}^{1}\ . \tag{24}$$

Any smooth function h which is one at $x=\pm 1$ and satisfies this relation for all such v is, in fact, a solution of Eq. (7) with boundary conditions (11) as well.

Let $\mathcal{M}$ be the Hermite cubic polynomials [13] over a given partition,

$$-1=x_0<x_1<\cdots<x_K=1\ ,$$

of $(-1,1)$; i.e., $\mathcal{M}$ is the set of all C^1 piecewise cubic polynomials. Take $\mathcal{M}_0$ to consist of those functions in $\mathcal{M}$ which vanish at both ends of the interval $(-1,1)$. The space $\mathcal{M}$ has dimension $2(K+1)$ and it is conveniently parametrized by the values of the function and its derivative at the mesh points x_i. If $w\in\mathcal{M}$, then

$$w(x)=\sum_{i=0}^{K}[w(x_i)v_i(x)+w_x(x_i)s_i(x)]\ ,$$

where with $\Delta x_j=x_{j+1}-x_j$ and $I_j=(x_j,x_{j+1})$

$$v_i(x)=\begin{cases}V_0\left[\dfrac{x-x_i}{\Delta x_i}\right], & x\in I_i\\ V_1\left[\dfrac{x-x_{i-1}}{\Delta x_{i-1}}\right], & x\in I_{i-1}\\ 0 \text{ otherwise}\ ,\end{cases}$$

$$s_i(x)=\begin{cases}\Delta x_i S_0\left[\dfrac{x-x_i}{\Delta x_i}\right], & x\in I_i\\ \Delta x_{i-1}S_1\left[\dfrac{x-x_{i-1}}{\Delta x_{i-1}}\right], & x\in I_{i-1}\\ 0 \text{ otherwise}\ ,\end{cases}$$

$$V_0(x)=1-3x^2+2x^3\ ,$$

$$V_1(x)=3x^2-2x^3\ ,$$

$$S_0(x)=x(x-1)^2\ ,$$

$$S_1(x)=x^2(x-1)\ .$$

The mesh points $\{x_i\}$ are chosen symmetrically about 0, and the mesh was chosen to be extremely refined in the areas in which the singularity develops. We also imposed the constraint

$$\tfrac{1}{2}\le\frac{\Delta x_i}{\Delta x_{i+1}}\le 2\ .$$

The continuous-time Galerkin approximation is a differentiable function $H(t)$ taking values in $\mathcal{M}$; where it is convenient, think of H as being $H(x,t)$. The defining relation for H are

$$\begin{aligned}&(H_t,v)+G(H,H,v)=Pv_x|_{-1}^{1},\quad v\in\mathcal{M}_0\ ,\\ &H(-1,t)=H(1,t)=1\ ,\\ &H(x,0)\in\mathcal{M}\text{ given}\ ,\end{aligned} \tag{25}$$

where

$$\begin{aligned}&(\varphi,\psi)=\int_{-1}^{1}\varphi\psi dx\ ,\\ &G(\varphi,\psi,v)=\int_{-1}^{1}\varphi_{xx}(\psi v_x)_x dx\ .\end{aligned} \tag{26}$$

Expressed in the above basis for $\mathcal{M}$, Eq. (25) becomes a system of $2K$ ordinary differential equations in $2K$ variables.

These relations are discretized in time using a finite-difference method as described below. Let

$$0=t^0<t^1<\cdots$$

be an increasing sequence of times. We compute a sequence $\{H^n\}$ of functions in $\mathcal{M}$ where H^n approximates $H(t^n)$.

Adopt the notation

$$\Delta t^{n+1}=t^{n+1}-t^n ,$$
$$\partial_t H^{n+1}=(H^{n+1}-H^n)/\Delta t^{n+1} , \tag{27}$$
$$H^{n,\theta}=\theta H^{n+1}+(1-\theta)H^n ,$$
$$\tilde{H}^n=\begin{cases} H^n+\dfrac{\Delta t^{n+1}}{2\Delta t^n}(H^n-H^{n-1}), & n>0 \\ H^0, & n=0 . \end{cases}$$

Given $H^0\in\mathcal{M}$, the sequence $\{H^n\}$ for $n>0$ is defined by the following relations:

$$(\partial_t H^{n+1},v)+G(H^{n,\theta},\tilde{H}^n,v)+G(\tilde{H}^n,H^{n,\theta}-\tilde{H}^n,v) = Pv_x|_{-1}^{1}, \quad v\in\mathcal{M}_0 , \tag{28}$$
$$H^n(-1)=H^n(1)=1 .$$

For $\theta=\frac{1}{2}$ this is a second-order correct implicit method based on the trapezoidal rule with extrapolation for some of the nonlinearities. The scheme is still second-order correct (for $\theta=\frac{1}{2}$) if the second $G(\ )$ term is omitted, but it was found empirically that omitting that term induced a strong time-step limitation.

In our numerical experiments with this method, the initial data and the mesh were taken to be symmetric about 0; this makes H^n an even function for each n. For efficiency the symmetry was enforced on the computed solution. Also we used θ slightly larger than $\frac{1}{2}$ to damp very-high-frequency modes.

The initial time step was chosen experimentally and an *ad hoc* time-step adjustment rule controlled the step thereafter. The step adjustment rule rejected steps on which the minimum of H decreased by more than 10%; in these cases the step size was halved and the step was retried. After long periods without step rejection modest step increases were tried, subject to a predefined maximum. Based on repeated experiments with various time-step constraints, it seems that the time truncation was small relative to the space truncation.

In experiments in which H is actually getting very small, we computed with the difference between H and the candidate for the limiting steady-state solution. This was done to minimize the effects of rounding error.

In all our experiments to date the mesh $x_0,\ldots,x_K$ was held fixed in time. The mesh was far from uniform in space in most cases.

In order to understand the nature of the computed solutions, we need to examine not only the values of the solution, but certain derivatives as well. The current $J=hh_{xxx}$ is of particular importance. The technique that we use to approximate the value of the current is adapted from an idea of John Wheeler, and we will describe it in the continuous-time case. Let y be a given point in $(-1,1)$ and suppose that $v\in\mathcal{M}_0$ is such that $v(y)=1$ and $v_x(y)=v_x(1)=0$. The current at (y,t) is computed as follows:

$$J(y)=\int_y^1 [H_t v+H_{xx}(Hv_x)_x]dx . \tag{29}$$

The integral above can be computed on a single subinterval, since shifting v by any element of $\mathcal{M}_0$ which is only nonzero in $(y,1)$ does not change the computed value. The current at the end points is computed in a similar way. Once the current is known we have a natural approximation of h_{xxx}.

III. RESULTS OF SIMULATION

In this section, we discuss the numerical solutions. From the argument of Sec. II B, one should expect that these simulations of fluid flow will show very different results in two cases: For P sufficiently small, there will be a "dull" behavior in which the pressure in the fluid

$$p(x,t)=P-h_{xx} \tag{30}$$

goes to a constant value, 0, as time goes to infinity. Then, h will approach the smooth function defined by Eq. (17).

The prototype of this kind of behavior occurs at $P=0$. In this case, h remains one for all times. We will argue that a smooth approach to the profile (17) probably holds for all $P<2$. In Figs. 4 and 5 we plot our numerical solution for one of these "dull" cases, $P=1$. The solution does indeed seem to approach the asymptotic behavior shown in Eq. (17).

The time dependence of the solution depicted in Figs. 4 and 5 can be reasonably well understood. As the fluid flows out of the cell, the curvature of the interface increases throughout. Some pressure gradient is maintained, in which higher pressures are found toward the center of the cell, and this pressure gradient pumps fluid out of the cell. The gradient is gradually reduced as fluid leaves the cell, so that at large times the pressure is al-

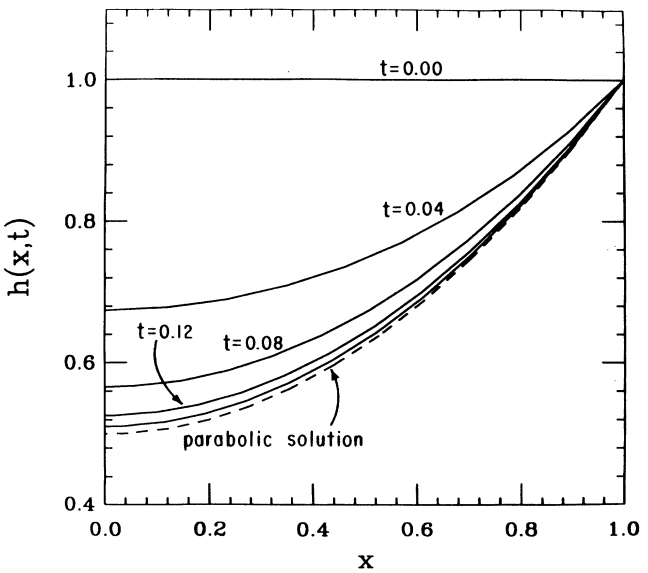

FIG. 4. The behavior of $h(x,t)$ in the case $P=1$. Here $h(x,t)$ never will become singular. The solution for $h(x,t)$ is shown for selected times. Only the region $0<x<1$ is shown because the curves are symmetrical about $x=0$. The dashed curve is the parabolic equilibrium solution of Eq. (7).

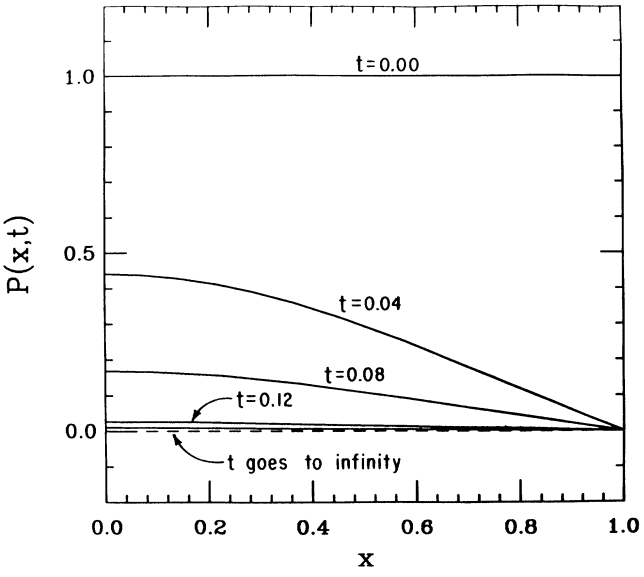

FIG. 5. The behavior of $p(x,t)$ in the case $P=1$. Here $p(x,t)$ never will become singular. The solution for $p(x,t)$ is shown for selected times. Only the region $0<x<1$ is shown because the curves are symmetrical about $x=0$. The dashed curve is the parabolic equilibrium solution of Eq. (7).

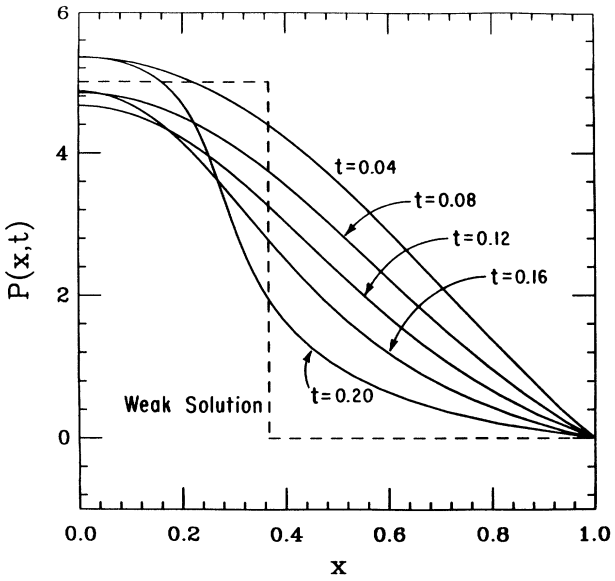

FIG. 7. The pressure $p=P-h_{xx}$ at selected times for the $P=5$ case.

most constant and the flow ceases.

Thus we know what can happen for $P<2$. But what do we expect for $P>2$?

To see what happens in the early stages of the flow, look at Figs. 6 and 7, which give the simulation for $P=5$. Figure 6 shows an h which gradually goes down and

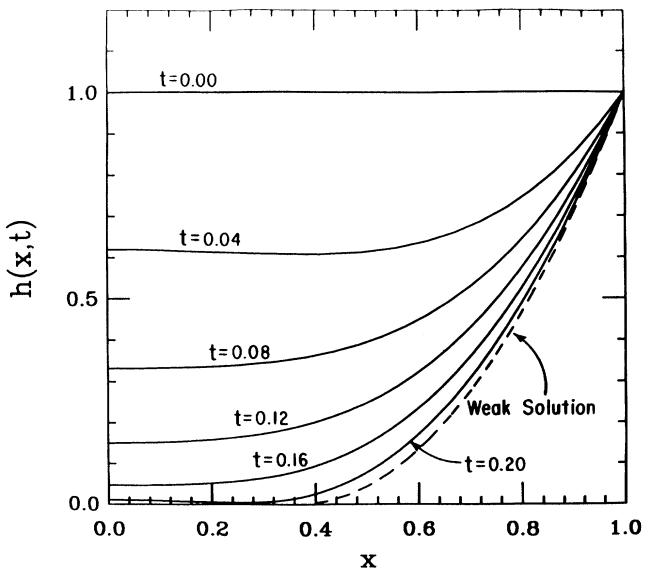

FIG. 6. The solution for $h(x,t)$ is shown for selected times for the $P=5$ case. Only the region $0<x<1$ is shown because the curves are symmetrical about $x=0$. The dashed curve is the weak solution of Eq. (7).

seems to more or less approach the dashed curve marked "weak solution." Thus, here too, h does seem to have some tendency to approach a time-independent solution.

But, if we look more carefully at Fig. 6, we can see some very interesting details. Over the earlier times, $t\leq 0.16$, h decreases monotonically as one approaches the center of the cell. The plots look qualitatively similar to the ones shown for $P=1$. But, toward the end of the time interval shown in Fig. 6, something new happens. In the last two curves, h shows a tendency to flatten out toward the center, and even at the last time to show a minimum for x bigger than zero. To understand this behavior, notice that at time 0.16, the "curvature" h_{xx} has an average value of order 3 or so over the outer portions of the cell. Hence the pressure is relatively small in these outer portions. But towards the center h_{xx} must remain small, since h cannot become negative. Thus the pressure rises to get close to the value 5 near the center. There is then a very substantial gradient of pressure in the region $0.2<x<0.5$. This gradient pumps fluid to larger x, out of that region. By the time 0.2, a minimum of the height has appeared near $x=0.25$. Now, the height and its second derivative remain small for all x between 0 and 0.25. Correspondingly, there is a large pressure gradient between x of 0.2 and 0.3. Fluid now is pumped out of this region, toward larger x, and the minimum of h moves to the right. Thus, in the course of the simulation, fluid is being continually pumped out of the region in which $x<x_0=0.36754\ldots$, particularly near the maximum gradient of p, which is also close to the minimum in h.

We can perceive two different eras in the flow. In the first era, for $t\lesssim 0.2$, h is monotone increasing from the center to the outside. In the second era, $t\gtrsim 0.2$, we see a minimum (or pinch) in h for nonzero x. This situation is

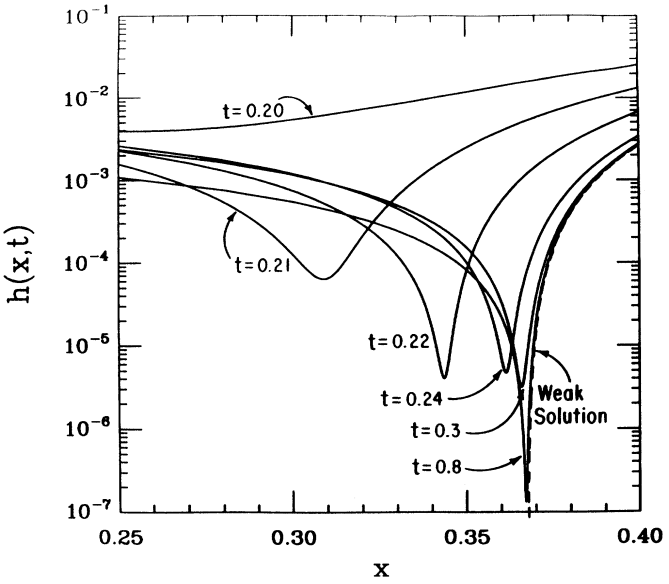

FIG. 8. A blowup of the small h region of the $P=5$ case carried to later times.

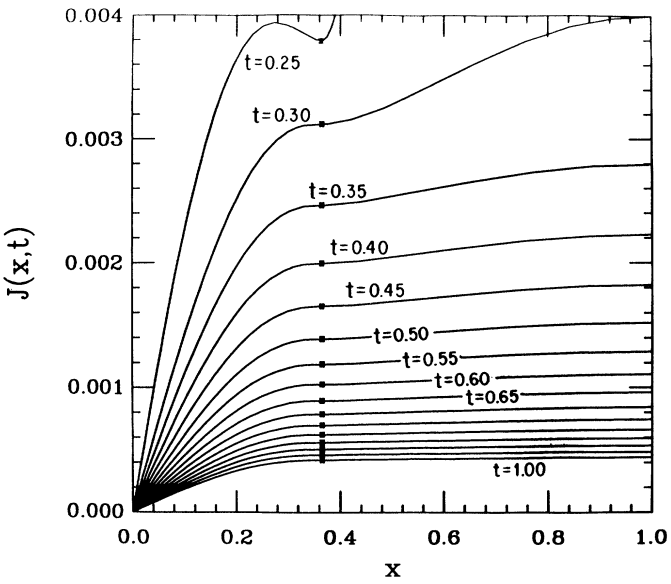

FIG. 10. The current hh_{xxx} at various times for $P=5$. The boxes on the current curves are the minimum positions of h at those times.

depicted in Fig. 8. In the period depicted, the simulation shows a pronounced minimum in height $h_{\min}$ at a pinch point $x^*(t)$. As time goes on, at least after $t=0.24$, $h_{\min}$ becomes smaller and smaller while $x^*(t)$ approaches x_0. Note how, as t increases, the right-hand portion of the solution for h approaches the quadratically varying weak solution.

Figure 8 indicates that in the later era there are three regions of x, each with its own characteristic behavior. This delineation is very clearly shown in Fig. 9, which plots the pressure as a function of time. In the outer region, the pressure is almost zero and h_{xx} is almost P.

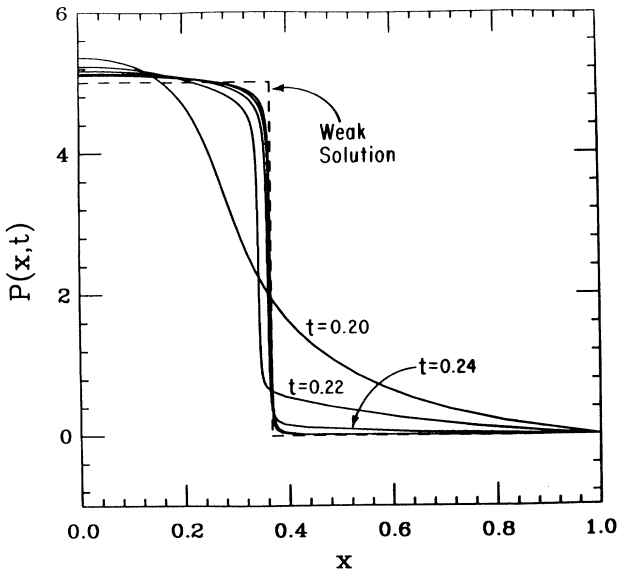

FIG. 9. The pressure at selected late times for $P=5$.

Next there is a pinch region in which the pressure varies very rapidly. The width of this region rapidly decreases as a function of time. In the pinch h is very, very small and reaches a minimum $h_{\min}(t)$ at x equal to $x^*(t)$. As one can see from Fig. 10, x^* lies in the middle of the pinch region. Lastly, there is a central region in which h has a weak maximum at $x=0$. The pressure is just a bit above P in the region. We call the value of h at this maximum $h_0(t)$. As t increases, the flow of current moves the pinch region outward and reduces the amount of fluid in the central region. However, the small value of h in the pinch prevents the system from producing a large current, and thereby keeps the time-variation slow.

Figure 10 shows the behavior of the current. After $t=0.40$, the current rises almost linearly through the central region and varies weakly through the outer region. Through the pinch region the current is substantially constant. As we shall see, this constancy implies a simple and universal behavior for h near the pinch.

IV. SCALING AND UNIVERSALITY

We systematically plot the various quantities of interest in the second era as a function of time. There are two important heights: h_0, which is the height at the center, and the minimum height $h_{\min}$. Figure 11 shows these heights, in log-log plots against t. Straight lines on these plots would represent power law behavior in time. The average slopes on these plots are of order -0.98 and -3.9, representing, respectively, situations in which h_0 behaves as $t^{-0.98}$ while $h_{\min}$ varies roughly as $t^{-3.9}$. But, there is a slight downward curvature of these curves, which suggests that the powers are slightly larger in magnitude than the one stated. In addition, the ratios

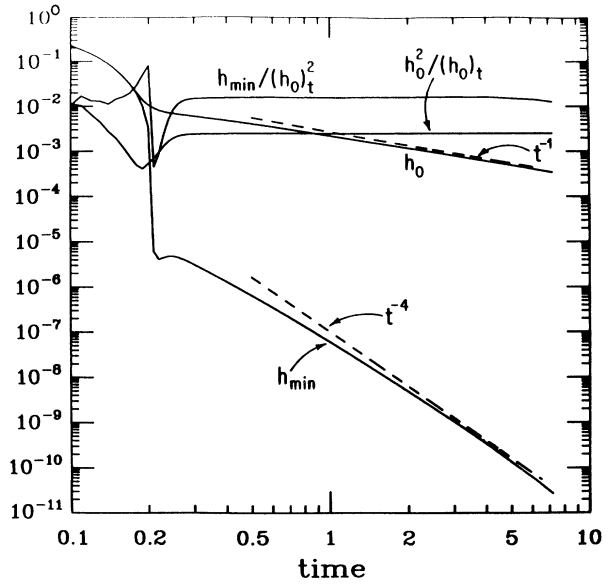

FIG. 11. The minimum of h, $h_{\min}(t)$, the central value h_0, the ratios $h_{\min}/(h_0)_t^2$ and $h_0^2/(h_0)_t$ are plotted as functions of t. The least-squares power-law fits have, respectively, the slope -0.98 for h_0 and -3.9 for $h_{\min}$. The two dashed lines show the theoretical predications.

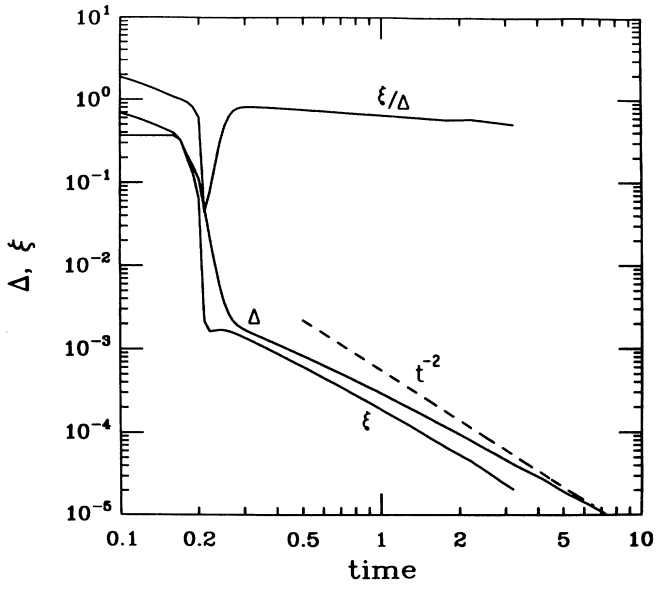

FIG. 12. Some distance plotted against time. We show Δ, the displacement of the pinch point from its weak solution value, and the characteristic thickness of the pinch region ξ plotted as a function of t. Notice that Δ falls as the -1.75 power of t and ξ varies as the -1.87 power of t. Notice the apparently simple scaling behavior of these quantities and the apparent constancy of the ratio ξ/Δ.

$$R_1=\frac{h_{\min}}{(h_0)_t^2}\ ,$$

$$R_2=\frac{h_0^2}{(h_0)_t}$$

seem to be very accurately constant for large t. These results suggest that the solutions show a scaling behavior in which $h_{\min}$ and h_0, respectively, vary as $1/t$ and $(1/t)^4$.

We look for additional scaling. In Fig. 12, we plot the time dependence of some characteristic distances. There are two important lengths in this problem. The first,

$$\Delta(t)=x_0-x^*(t)\ , \tag{31}$$

is the distance between the pinch point and the position of the putative asymptotic singularity. Thus it measures a shift in position of the pinch point. The other length, ξ, is introduced as a measure of the thickness of the pinch region. It is defined to be the distance over which the height doubles from its minimum value:

$$2=\frac{h(x^*(t)+\xi(t),t)}{h_{\min}}\ . \tag{32}$$

From Fig. 12, we see that Δ varies roughly as $t^{-1.75}$, with ξ varying roughly as $t^{-1.87}$, and the ratio Δ/ξ being rather time independent. There is one more scaling relation which will prove important in what follows, the scaling of the current. Let $J(t)$ be the current $j(x,t)$ evaluated at the minimum of h. Figure 13 plots $J(t)$ versus t, showing that J decreases roughly as t^{-2}, and also gives a plot which shows that $J(t)/(h_0)_t$ is roughly constant.

The plots of Figs. 11–13 suggest that there might be a scaling behavior shown by the solutions. We look for this scaling, since it might well give us insight into the possible infinite-time structure of the solutions.

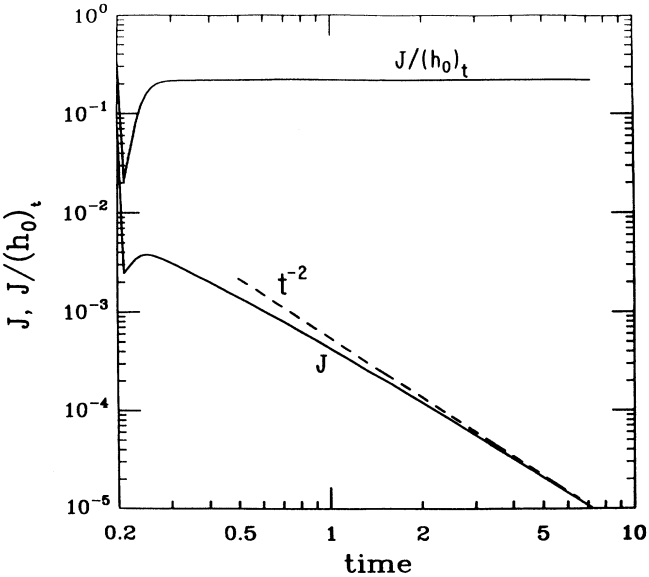

FIG. 13. Scaling of the current. The current at the pinch point $J(t)$ is plotted versus t and also $J/(h_0)_t$ is shown roughly to be a constant.

A. Similarity solutions

Since in the $P>2$ case Eq. (7) does not have any static solution, one might expect that $h(x,t)$ has a similarity solution for late time. Hopefully this will enable us to explain various scaling relations obtained from our numerical simulations.

Assume that the late-time solution of Eq. (7) has a similarity solution of the following form:

$$h(x,t)=\chi(t)G\left[\frac{x-x_c-\gamma[\chi(t)]^{\delta}}{\beta[\chi(t)]^{\alpha}}\right], \tag{33}$$

where x_c, α, β, γ, and δ are constants. Putting this solution into Eq. (7), if we demand that functions G and χ can be separated, we must have $\gamma=0$ or $\delta=\alpha$. Now we have two separate equations for G and χ:

$$(GG_{\eta\eta\eta})_{\eta}-\lambda\left[G-\alpha\eta G_{\eta}-\frac{\delta\gamma}{\beta}G_{\eta}\right]=0, \tag{34}$$

$$\beta^4\chi_t+\lambda\chi^{2-4\alpha}=0, \tag{35}$$

where

$$\eta=\frac{x-x_c-\gamma[\chi(t)]^{\alpha}}{\beta[\chi(t)]^{\alpha}},$$

and λ is an adjustable constant. Further, we set $G(0)=1$ so that

$$h(x_c+\gamma[\chi(t)]^{\alpha},t)=\chi(t).$$

In the central region, G is a symmetric function of x. So $x_c=0$, $\gamma=0$, and $\chi(t)=h_0$. For late time there is a very natural scale for $x-x_0$ which roughly defines the boundary of the central region. This makes $\alpha=0$ and $\gamma=0$ a very natural choice for the similarity solution of $h(x,t)$ in the central region. From Eq. (35) we immediately see that

$$\chi_t\sim\chi^2$$

or

$$(h_0)_t\sim h_0^2,$$

and for late time G satisfies

$$\lambda G-(GG_{\eta\eta\eta})_{\eta}=0, \tag{36}$$

where η is x/x_0. This G function defines a universal shape in the central region when time is very large.

For the pinch region, the situation is different from that of the central region. Now the natural choice of $\chi(t)$ is $h_{\min}$. This requires $x_c+\gamma[\chi(t)]^{\alpha}=x^*$. Because $x^*\approx x_0$ for large t, we set $x_c=x_0$. Now Δ defined in Eq. (31) is x^*-x_c or $\gamma[\chi(t)]^{\alpha}$. The ξ defined in Eq. (32) is the scale of the size of the pinch region, or $\xi=[\chi(t)]^{\alpha}$. In Fig. 12 one can see that ξ/Δ approaches a constant for large time. This fact indicates that the larger the time is, the better our similarity assumption becomes. When time gets very large, $h_{\min}$ becomes very small and so does the time derivative of $h(x,t)$. If α is not less than $\frac{1}{4}$, we have to set λ to be zero. We will see that this is indeed the case in our simulation. From simulation results we can estimate that α is about $\frac{1}{2}$. Now the shape of the interface in the pinch region is determined by

$$(GG_{\eta\eta\eta})_{\eta}=0 \tag{37}$$

or

$$(hh_{xxx})_x=0. \tag{38}$$

B. Universality in central region

To check whether our similarity solution works in the central region, we plot function g, which is defined as

$$g(z,t)=\frac{h(zx_0,t)}{h_0}. \tag{39}$$

If there is a universality in the central region, we should expect the g defined by Eq. (39) to be essentially independent of time. From Fig. 14 we can see that $g(z,t)$ does change with time very slowly for $t\geq 0.5$. So for late times, the function $g(z,t)$ will approximately be the G defined in Eq. (33), which satisfies Eq. (36).

Figure 14 also shows the comparison between the g function obtained from late-time simulation results and a numerical solution G of Eq. (36) with boundary conditions

$$G(0)=1,\quad G_{\eta}(0)=0,$$

$$G_{\eta\eta}(0)=-2.836,\quad G_{\eta\eta\eta}(0)=0,$$

and the constant λ in Eq. (36) is set to be 7.000. All curves agree with each other very well. So for the central region, we can safely set the index α defined in Eq. (33) to zero. This gives us a scaling relation between h_0 and h_{0t}:

$$(h_0)_t\sim h_0^2. \tag{40}$$

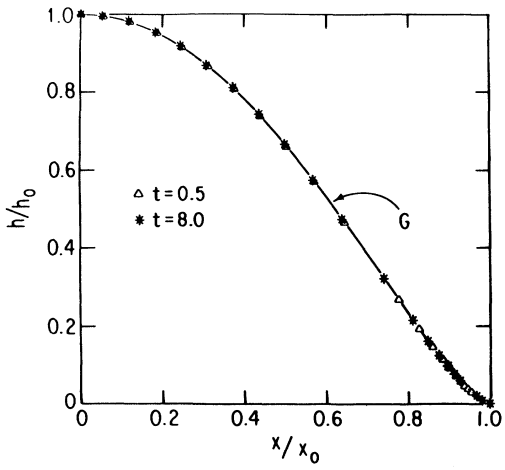

FIG. 14. Comparison between the G function for $t=0.5$–8.0 of the central region and a numerical solution of Eq. (3.12) using the initial conditions $G(0)=1$; $G_{\eta}(0)=0$; $G_{\eta\eta}(0)=-2.836$; $G_{\eta\eta\eta}(0)=0$; and $\lambda=7.00$. From our simulation result we know that g changes with time very slowly when $t>0.5$.

From Fig. 11 one can see that h_0^2/h_{0t} approaches a constant for large times.

C. Universality in pinch region

According to Fig. 9, once h has gotten very small, it stops varying very rapidly. This result suggests that in the pinch region, we can analyze the behavior of h in the region of the minimum by using Eq. (38). Then, the current is constant in this region, so that we can write

$$hh_{xxx}=J(t) . \tag{41}$$

We focus on the region near the positive $x^*(t)$, where J is positive. We now pause for a reasonably full analysis of the most relevant solutions to Eq. (41). We consider a situation in which h is small near the minimum and varies rapidly over a distance scale $\xi(t)$ around the minimum at $x^*(t)$. Thus we choose

$$h(x,t)\approx F\left[\frac{x-x^*(t)}{\xi(t)}\right]h_{\min} . \tag{42}$$

Equations (41) and (42) together imply that $F(y)$ obeys

$$FF_{yyy}=1 . \tag{43}$$

The constant in Eq. (3.3) is given the value unity when we make the particular choice

$$J=h_{\min}^2\xi^{-3} .$$

One integration of Eq. (43) gives

$$FF_{yy}-\tfrac{1}{2}F_yF_y=y-A , \tag{44}$$

where $A(t)$ is another integration constant. For large y, we demand that $h(x,t)$ fit into the weak solution. For this reason we choose F to have the asymptotic behavior

$$F(y)\to\tfrac{1}{2}y^2 \text{ as } y\to\infty . \tag{45}$$

We lose no generality with this choice, and simply use it to define $\xi(t)$ in terms of J. Recall form (18) of the weak solution and fit Eqs. (42) and (45) onto that weak solution by demanding

$$\sqrt{J(t)/\xi(t)}=P . \tag{46}$$

Equation (44) admits three possible behaviors of $F(y)$ as y goes to minus infinity. In one case, F can grow as y^2. We reject this case because we wish to have h quite small to the left of the pinching point. Other solutions attain $F=0$, and then permit no continuation past the point of this occurrence. These are also rejected. Finally, there is an exceptional solution in which

$$F(y)\to\sqrt{8/3}(A-y)^{3/2} \text{ as } y\to-\infty . \tag{47}$$

Figure 15 plots this particular solution. We normalize the solution in exactly the same way as we normalized the experimental data. Specifically we take the minimum of F to be at $y=0$ and demand

$$F(0)=1, \quad J(0)=F(0)F_{yyy}(0)=1 . \tag{48}$$

On the same plot, we show the actual result of the simulation for $P=5$, given in terms of

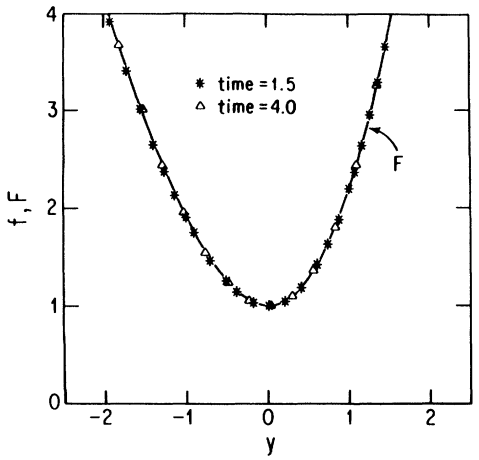

FIG. 15. Comparison between the numerical solutions in pinch region at $t=1.5$ and 4.0 and the universal form F.

$$f(y,t)=\frac{h(x^*+(h_{\min}^2/J)^{1/3}y,t)}{h_{\min}} . \tag{49}$$

This $f(y,t)$ has been defined to have the value one at $y=0$ and

$$f(0,t)f_{yyy}(0,t)=1 ,$$

just like F. If our theoretical argument is correct, f should be time independent, and, in fact, exactly the same as F. The plot supports these statements.

According to the results just derived, if we but knew the current $J(t)$, we would know the entire solution in the pinch region. But now we can argue in a heuristic fashion that since the current carries mass out of the central region, and since the central region has mass which is of the order h_0 times the almost fixed size of the central region, then

$$J\sim(h_0)_t .$$

From this argument we would conclude that the various constants describing the pinch region scaled as

$$\xi\sim J\sim(h_0)_t, \quad h_{\min}\sim(h_0)_t^2 . \tag{50}$$

The plots seem to bear out these contentions. Thus, we can argue that we do seem to understand the pinch region reasonably well.

V. CONCLUSIONS

In this paper we have studied the droplet-breakup problem in a Hele-Shaw cell. A simplified equation is derived for the width of a thin neck between two masses of the fluid from a lubrication approximation. This equation can be used to describe the singularity-developing process in the droplet-breakup problem in a Hele-Shaw

cell. Starting from certain smooth initial flows, we have found solutions to the simplified equation which apparently will not reach zero in finite time. This means that, under these conditions, droplet breakup cannot happen in finite time in a Hele-Shaw cell. For late time, the minimum width of the thin neck decreases like $1/t^4$. Similarity solutions are found for the late-time shape of the interface in the pinch and central regions. Comparison between the simulation results and theoretical universal shapes is made and the agreements are very satisfying. Further investigation of this problem with various initial and boundary conditions is being pursued (see [14]) to see under what conditions one can expect finite-time singularities.

ACKNOWLEDGMENTS

This research was supported in part by the ONR, the University of Chicago MRL, NSF Grant No. CHE 91-06240, the A. P. Sloan Foundation (R.E.G.), and NSF Grant No. DMS-915792 (M.J.S.). We would like to thank A. Bertozzi, M. Brenner, J. Lebowitz, M. Marder, A. I. Pesci, M. Pugh, H. Rachford, L. Schwartz, and G. Vasconcelos for helpful discussions.

[1] P. Bleher, J. L. Lebowitz, and E. R. Speer (unpublished).
[2] J. Weiss, J. Math. Phys. **24**, 1405 (1983).
[3] A. J. Chorin, Commun. Math. Phys. **83**, 517 (1982).
[4] R. E. Goldstein, T. G. Mason, and E. Shyamsunder (private communication).
[5] H. S. S. Hele-Shaw, Nature **58**, 34 (1898).
[6] R. E. Goldstein, T. G. Mason, and E. Shyamsunder (private communication).
[7] These tales were told to one of us by Hassam Aref, who said that they had the status of old wives' tales.
[8] See example, J. W. Maclean and P. G. Saffman, J. Fluid Mech. **102**, 455 (1981); C. W. Park and G. M. Holmsey, *ibid.* **139**, 291 (1984); D. A. Reinelt and P. G. Saffman, SIAM J. Sci. Stat. Comput. **6**, 542 (1985); D. A. Reinelt, J. Fluid. Mech. **183**, 219 (1987).
[9] D. Bensimon, L. P. Kadanoff, S. Liang, B. I. Shraiman, and C. Tang, Rev. Mod. Phys. **58**, 977 (1986).
[10] P. G. Saffman and G. I. Taylor, Proc. R. Soc. London, Ser. A **245**, 312 (1958).
[11] A. Cameron, *Principles of Lubrication* (Longmans, London, 1966).
[12] R. Courant and D. Hilbert, *Methods of Mathematical Physics* (Interscience, New York, 1953), Vol. II.
[13] G. Strang and G. J. Fix, *An Analysis of the Finite Element Method* (Prentice-Hall, Englewood Cliffs, NJ, 1973).
[14] T. F. Dupont, R. Goldstein, L. P. Kadanoff, and S. Zhou (unpublished).